*J. Fluid Mech.* (1980), *vol.* 98, *part* 4, *pp.* 673–701
*Printed in Great Britain*



# Surface-roughness effects on the mean flow past circular cylinders

By O. GÜVEN

Endem İnsaat, Büyükdere Caddesi Yonca B Blok 121/22, Levent, Istanbul, Turkey

C. FARELL

St Anthony Falls Hydraulic Laboratory, University of Minnesota, Minneapolis, Minnesota 55414

AND V. C. PATEL

Institute of Hydraulic Research, University of Iowa, Iowa City, Iowa 52242

(Received 16 June 1976 and in revised form 24 May 1979)

Measurements of mean-pressure distributions and boundary-layer development on rough-walled circular cylinders in a uniform stream are described. Five sizes of distributed sandpaper roughness have been tested over the Reynolds-number range $7 \times 10^4$ to $5{\cdot}5 \times 10^5$. The results are examined together with those of previous investigators, and the observed roughness effects are discussed in the light of boundary-layer theory. It is found that there is a significant influence of surface roughness on the mean-pressure distribution even at very large Reynolds numbers. This observation is supported by an extension of the Stratford–Townsend theory of turbulent boundary-layer separation to the case of circular cylinders with distributed roughness. The pressure rise to separation is shown to be closely related, as expected, to the characteristics of the boundary layer, smaller pressure rises being associated with thicker boundary layers with greater momentum deficits. Larger roughness gives rise to a thicker and more retarded boundary layer which separates earlier and with a smaller pressure recovery.

## 1. Introduction

An understanding of the influence of surface roughness on the flow around circular cylinders is important not only because of the fundamental flow phenomena involved but also because of the significance of surface-roughness effects in several practical applications. For example, important reductions in the magnitude of the mean peak suction on cooling tower shells can be obtained if the surface is roughened by external ribs (Niemann 1971; Farell, Güven & Maisch 1976). The effects of roughness also play a decisive role in the wind-tunnel modelling of the wind loading on rounded structures (Farell 1971; Batham 1973; Szechenyi 1975; Farell, Güven & Patel 1976). However, there have been only a few fundamental studies reported in the literature on the influence of surface roughness on the flow past bodies, and these studies have been exclusively experimental. For circular cylinders with surface roughness, major references are Fage & Warsap (1929), Achenbach (1971, 1977) and Szechenyi (1974,

0022–1120/80/4460–8920 $02.00 

1975). With the exception of Achenbach's results, most of the information given in these studies is in terms of drag and lift coefficients only, and the interrelationship between mean-pressure distributions and the boundary-layer development has not been studied in detail. Furthermore, there are conflicting conclusions in the literature regarding the effects of surface roughness at large Reynolds numbers.

This paper presents the results of an experimental and analytical investigation undertaken to clarify the influence of surface roughness on the mean pressure distributions. The experiments include measurements of pressure distributions on cylinders with sandpaper roughness over the Reynolds-number range $7 \times 10^4$ to $5{\cdot}5 \times 10^5$ in a uniform stream and boundary-layer measurements at two supercritical Reynolds numbers. The analytical study consisted of calculations of the boundary-layer development using a simple integral method and an extension of the Stratford–Townsend theory of turbulent boundary-layer separation, the details of which have been described elsewhere (Güven, Patel & Farell 1977). The theory and the calculations are compared here with experimental data and are used in the discussion of the roughness effects.

The experimental arrangement is described in § 2 and the results are presented in § 3. In § 4 the results are discussed in the light of the present and previous experimental and analytical studies of the boundary-layer behaviour, with particular emphasis on the effects of roughness at large Reynolds number. In view of the apparently contradictory conclusions in the literature as to the effects of roughness at large $Re$, a detailed examination of previous experimental results has been included in this section. The discussion leads to some novel conclusions and clarifies certain observations made by earlier investigators. It is shown that the influence of roughness on the pressure distributions is present even at large Reynolds numbers. The interrelationship between the characteristics of the boundary layer and the pressure distribution has been explored and it is concluded that the observed roughness effects have their origin in the influence of roughness on the development and separation of the boundary layer.

## 2. Experimental arrangement and instruments

### 2.1. *Wind tunnel*

The experiments were conducted in the largest closed-circuit wind tunnel of the Iowa Institute of Hydraulic Research. For the present study, an additional contraction and a corresponding diffuser were added to the 7·3 m long working section of the tunnel to change the original 1·52 m octagonal cross section to a nearly rectangular cross section 1·52 m wide and 0·834 m high. Mean velocity distributions were measured at several sections along and across the tunnel ahead of the cylinder. The maximum cross-sectional variations in the approach velocity, $V_0$, were less than 1·2 % (mostly less than 0·5 %) of the mean over the traversed area. A point where the reference static and total pressures could be measured was chosen on the basis of the longitudinal traverses ahead of the model. The free-stream turbulence intensity (r.m.s. axial velocity fluctuation divided by $V_0$) was less than 0·2 %.

### 2.2. *Model, mountings and alignment*

Two 27·05 cm diameter circular cylinders were used. The cylinders were turned from an aluminium pipe of 27·30 cm nominal diameter, and were built in two sections to

| Commercial name of sand paper | Grit no. | $k$ (mm) | $k_s$ (mm) | $k/d \times 10^3$ | $k_s/d \times 10^3$ |
|---|---|---|---|---|---|
| NORTON-Resinall, Adalox Paper, Closekote Aluminium Oxide | 40 | 0·430 | 0·675 | 1·59 | 2·50 |
| NORTON-Resinall, Adalox Paper, Closekote Aluminium Oxide | 36 | 0·535 | 0·840 | 1·98 | 3·11 |
| NORTON-Resinall, Durite Cloth, Type 3, Closekote Aluminium Oxide | 24 | 0·720 | 1·130 | 2·66 | 4·18 |
| 3M-Resinite, Floor Surfacing Paper, Type F Sheets, Open Coat | 20–3–1/2 | 0·960 | 1·130 | 3·55 | 4·18 |
| 3M-Resinall, Floor Surfacing Paper, Type F Sheets, Open Coat | 12–4–1/2 | 1·680 | 1·680 | 6·21 | 6·21 |

TABLE 1. Distributed roughnesses.

facilitate the construction of the pressure taps. The joint between the sections was 36·8 cm above the midsection and was sealed with silicon grease. Care was taken to ensure that there was no offset or misalignment of the two sections at the joint. Fifty-three pressure taps were drilled at the midsection of each cylinder and additional pressure taps were provided on one of the cylinders at a total of four levels, $\pm$ 10·2 cm and $\pm$ 20·3 cm above and below the midsection, in order to assess the two-dimensionality of the flow. All pressure taps had a diameter of 1·02 mm. The cylinder was mounted vertically, with its axis on the tunnel centre-plane 119·1 cm from the end of the tunnel contraction, and spanned the total height of the test section. The length-to-diameter ratio, $l/d$, of the cylinder was therefore 3·08 and the blockage ratio, defined as the cylinder diameter divided by the test section width, $d/w$, was 0·178. The cylinder was supported at the bottom by a board underneath the tunnel floor and could be rotated around its axis on this board. Additional supports were provided outside the tunnel floor and ceiling to securely fasten the cylinder after its orientation relative to the stream direction was adjusted. The cylinder orientation was determined by rotating the cylinder until the pressure taps at $\theta = \pm 30°$ gave the same reading, $\theta$ being the meridional angle measured from the forward stagnation point.

### 2.3. *Surface roughnesses*

The distributed roughnesses used in this study were provided by commercial sandpaper which was carefully wrapped around the cylinder in two pieces, leaving a gap of 3·2 mm centred at the measuring midsection. Two-sided adhesive tape was used to stick the paper, with the seam located at the rear of the cylinder. The thickness of the various papers, together with the adhesive tape, varied from about 1 to 2 mm. The commercial names of the papers used and the average particle sizes, $k$, as quoted by the manufacturers, as well as the corresponding values of $k/d$, based on the smooth-cylinder diameter, $d$, are given in table 1. Also included in table 1 are estimates of the equivalent hydrodynamic roughness heights, $k_s$, for these sandpapers, and the corresponding values of $k_s/d$, obtained as follows.

Achenbach (1971) determined the equivalent roughness of his sandpapers from pressure-drop experiments in a square duct. The standard grit numbers of the sandpapers which gave $k_s/d = 4{\cdot}5 \times 10^{-3}$ and $1{\cdot}1 \times 10^{-3}$ were no. 40 and no. 120, respectively (private communication). Since $d = 150\,\text{mm}$ in Achenbach's case, one obtains $k_s/k = 1{\cdot}57$ for the no. 40 paper ($k = 0{\cdot}430\,\text{mm}$) and 1·43 for the no. 120 paper ($k = 0{\cdot}115\,\text{mm}$). These values of $k_s/k$, i.e. the ratio of the equivalent roughness height to the average particle size, are in good agreement with those observed elsewhere for similar sandpapers but with different grain sizes as may be seen from a table given by Feindt (1957). Indeed, the photographs of the sandpapers given by Feindt and those of the papers used here appear to be quite similar. Also, the sandpaper used by Achenbach to obtain $k_s/d = 4{\cdot}5 \times 10^{-3}$ and that corresponding to $k/d = 1{\cdot}59 \times 10^{-3}$ in the present study have the same standard grit number, namely 40. In view of this, the value of $k_s/k = 1{\cdot}57$ determined from Achenbach's tests has been used here to estimate the equivalent roughness heights shown in table 1 for the no. 40, 36 and 24 sandpapers.

For the two coarsest papers, the estimation of $k_s$ proved more difficult since little previous information was available on sandpapers with such sparsely spaced grains. However, subsequent experimental results showed that the variation of the drag coefficient as well as other pressure distribution parameters with Reynolds number, presented in § 4.1 (*a*), was practically the same for sandpapers no. 24 and 20-3-1/2. The same value of $k_s/d$ was therefore assigned to both. This implies that $k_s/k$ for the latter, more sparsely grained paper is 1·18. Although a similar value of $k_s/k$ may be appropriate for the no. 12-4-3/4 paper, it was taken simply as unity in the absence of any direct evidence.

The foregoing would indicate that the values of $k_s/d$ quoted subsequently are necessarily approximate. However, with the possible exception of the coarsest sandpaper mentioned above, the margin of error in $k_s/d$ is not expected to be more than 10 %.

### 2.4. *Instruments*

The mean-pressure data were obtained by means of the IBM 1801 Data Acquisition and Control System of the Iowa Institute of Hydraulic Research, in conjunction with a 48-terminal Scanco Scanivalve, a Statham Model-PM5TC differential pressure transducer, and a Dana Model-2850 V-2 amplifier with a low-pass filter set at 0·010 kHz bandwidth. The pressure tubing from the cylinder (about 2·2 m long), as well as the leads (about 2 m long) from a Pitot-static probe used to measure the reference static and total pressures, were connected to the terminals of the scanivalve. During each experiment, the terminals were scanned in succession at prescribed time intervals and the pressure signals were monitored, averaged and recorded by the IBM 1801 system. Before each series of experiments, the pressure-measuring system was calibrated statically to ensure its proper operation and to check the linearity of its response. The calibration was done by applying a known pressure to a scanivalve terminal, using a simple apparatus (see Güven, Patel & Farell 1975*a*, figures 9 and 10) designed to generate the desired calibration pressures. The dynamic pressure of the approach flow was continuously monitored during the experiments to ensure steadiness. The maximum variation of the reference dynamic pressure during each test period (about 4·5 minutes) was less than 2 %. The raw data was finally obtained from the IBM 1801 system in the form of punched cards and subsequently analysed on the IBM 360/65 computer of the University of Iowa Computer Center.

The boundary-layer measurements were made by means of a flattened hypodermic needle with an outside diameter of 0·51 mm. The size of the tip after flattening was 0·30 mm. The probe was supported by the traversing mechanism described by Patel, Nakayama & Damian (1974). With this mechanism it was possible to make traverses in the direction normal to the cylinder surface at any desired station between $\theta = 65°$ and $\theta = 120°$. The main rod of the traversing mechanism was provided with a screw drive, a scale, and a vernier so that the normal distance $y$ from the cylinder surface to the axis of the probe was adjusted from outside the tunnel and measured with a resolution of 0·30 mm. The origin of the normal distance was taken as the top of the roughness elements. The probe zero was set prior to each test with the aid of a very thin small piece of paper (less than 0·05 mm thick) placed as a spacer between the probe tip and the rough surface face. The experiments were limited to Reynolds numbers less than $3 \times 10^5$ in order to avoid the probe deflexions and vibrations observed at larger tunnel speeds. The total pressure from the boundary-layer probe was measured by means of an alcohol micromanometer with a resolution of 0·025 mm alcohol. The velocity in the boundary layer was obtained assuming that the pressure across the layer remains constant and equal to that observed on the cylinder.

## 3. Experimental results

### 3.1. *Mean-pressure distributions*

Mean-pressure distributions were obtained, over the Reynolds-number range $7 \times 10^4$ to $5{\cdot}5 \times 10^5$, with a smooth cylinder and the five different distributed roughnesses given in table 1. Complete tabulation as well as graphical presentation of all these experimental results can be found in Güven, Patel & Farell (1975*a*, *b*). Typical pressure distributions (uncorrected for blockage) obtained with the smooth cylinder and one of the distributed roughnesses are shown respectively in figures 1 and 2. The smooth cylinder experiments served, on the one hand, as a useful reference for the rest of the experiments, and on the other, to assess the degree of two-dimensionality of the flow (see figure 1) and to verify the experimental procedures. The rather low value, $-3{\cdot}2$, of the minimum pressure coefficient for the pressure distribution shown in figure 1 may at first appear surprising. This is very likely due to the value of the Reynolds number being just beyond the dip in the drag coefficient curve and to tunnel blockage. Blockage effects in the critical Reynolds number range have not yet been fully documented, but they seem to be very significant (see Richter & Naudascher 1976; Farell *et al.* 1977). It should be noted that a similarly low value, about $-3.3$, was reported by Fage (1929) (with blockage ratio = 0·186 and $Re = 3{\cdot}3 \times 10^5$).

The mean-pressure data have been analysed to evaluate the drag coefficient $C_d$ (by integration of the pressure distribution), the base pressure coefficient $C_{pb}$ (defined as the average of the nearly constant pressure coefficients in the wake region), the minimum pressure coefficient $C_{pm}$, the location $\theta_m$ of the minimum pressure coefficient and the approximate location $\theta_w$ of the beginning of the wake region, defined as suggested by Niemann (1971) (see sketch in figure 1). The wake angle $\theta_w$ was found to be useful both as a parameter characterizing the pressure distribution (see also Niemann 1971; Farell & Maisch 1974) and as a rough indicator of the mean location of separation, since separation usually occurs within a short distance downstream of $\theta_w$ (see figure 6 and Patel 1968, figure 2). The drag coefficient, the Reynolds number and the pressure

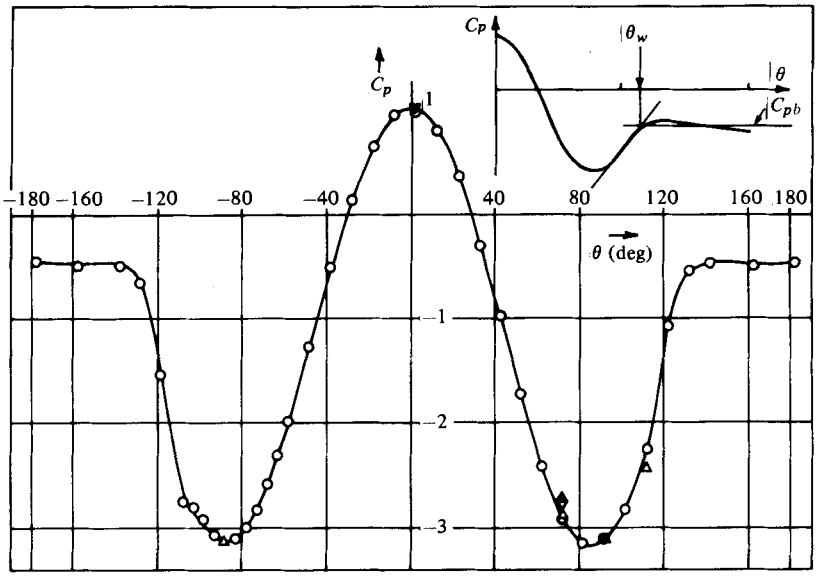


FIGURE 1. Smooth cylinder pressure distribution, $Re = 4{\cdot}1 \times 10^5$. Spanwise variations in pressure coefficient: ○, midsection; ▲, +20·3 cm level; △, +10·2 cm level; ▽, −10·2 cm level. Inset: definition of $\theta_w$.

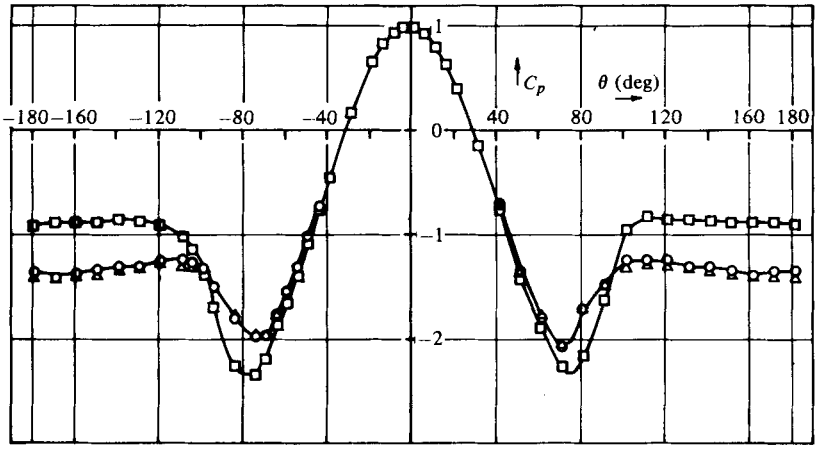


FIGURE 2. Pressure distributions on the cylinder with distributed roughness $k/d = 1{\cdot}59 \times 10^{-3}$. □, $Re = 1{\cdot}27 \times 10^5$; ○, $Re = 3{\cdot}10 \times 10^5$; △, $Re = 4{\cdot}14 \times 10^5$.

coefficients $C_{pm}$ and $C_{pb}$ have been corrected for blockage according to the procedure of Allen and Vincenti. The maximum corrections for $C_d$, $C_{pm}$ and $C_{pb}$ were, respectively, about 20, 21 and 24 % of the measured values. Recent experiments on cylinders with distributed roughness have supported the validity of this correction method in the region of Reynolds-number independence (Farell *et al.* 1977). The correction has been applied also in the region where the various parameters vary rapidly with the Reynolds number, although the application of this procedure in this region is somewhat doubtful, as also noted by Roshko (1961). Only the corrected values of $C_d$, $C_{pm}$ and $C_{pb}$ are con-

| Experiment | $\theta$ (deg) | $C_p$ | $\delta/d \times 10^3$ | $\delta_1/d \times 10^3$ | $\delta_2/d \times 10^3$ | $H = \delta_1/\delta_2$ |
|---|---|---|---|---|---|---|
| $Re = 3{\cdot}04 \times 10^5$, | 73 | $-1{\cdot}88$ | 14·6 | 4·96 | 2·52 | 1·97 |
| traverse at 2·5 cm | 83 | $-1{\cdot}73$ | 21·4 | 6·67 | 3·09 | 2·16 |
| above midsection | 93 | $-1{\cdot}54$ | 41·1 | 15·60 | 6·17 | 2·53 |
| | 98 | $-1{\cdot}46$ | 56·3 | 24·85 | 8·32 | 2·99 |
| $Re = 1{\cdot}5 \times 10^5$, at | 68 | $-1{\cdot}82$ | 10·1 | 2·38 | 1·55 | 1·54 |
| 2·5 cm above mid- | 73 | $-1{\cdot}87$ | 14·1 | 3·38 | 1·95 | 1·73 |
| section | 83 | $-1{\cdot}71$ | 17·5 | 5·08 | 2·85 | 1·78 |
| | 93 | $-1{\cdot}47$ | 33·2 | 11·94 | 5·19 | 2·30 |
| $Re = 1{\cdot}54 \times 10^5$, at | 73 | $-1{\cdot}85$ | 13·5 | 3·15 | 1·88 | 1·68 |
| 0·32 cm above mid- | 83 | $-1{\cdot}69$ | 18·0 | 4·83 | 2·62 | 1·84 |
| section | 93 | $-1{\cdot}47$ | 36·0 | 11·89 | 5·21 | 2·28 |

TABLE 2. Summary of boundary-layer parameters. $k/d = 2{\cdot}66 \times 10^{-3}$ ($k_s/d = 4{\cdot}18 \times 10^{-3}$).

sidered here unless otherwise noted. The results are presented and discussed together with the data of other investigators in § 4.

Some of the pressure distributions on the cylinder with distributed roughness exhibited a large asymmetry, in which case the values of $C_{pm}$, $\theta_m$ and $\theta_w$ were not evaluated. This was observed in three experiments with $k/d = 1{\cdot}59 \times 10^{-3}$ and in one experiment with $k/d = 1{\cdot}98 \times 10^{-3}$. It is interesting to note here that the asymmetric pressure distributions arise at the critical Reynolds numbers. Bearman (1969) also observed this feature on a smooth cylinder at the critical Reynolds numbers, and attributed to the asymmetric formation of the so-called 'laminar-separation and turbulent-reattachment bubble'. He also commented on the difficulty of maintaining a steady tunnel speed under these conditions. Similar problems were encountered in the present study during the four experiments referred to above, but since the pressure measurements on the opposite sides of the cylinder were not made simultaneously, it was not possible to draw a definitive conclusion concerning the origin of the observed asymmetry. Nevertheless, it was found that the mean pressures in the wake region remained remarkably constant even under these conditions. Both the base pressure coefficient and the drag coefficient were evaluated for these cases although $C_{pm}$, $\theta_m$ and $\theta_w$ were not.

### 3.2. *Boundary-layer velocity profiles*

Boundary-layer measurements were performed with one of the distributed roughnesses, $k/d = 2{\cdot}66 \times 10^{-3}$, for the two Reynolds numbers: $Re = 1{\cdot}54 \times 10^5$ and $3{\cdot}04 \times 10^5$. The velocity profiles are presented in figures 3(*a*, *b*) where $u$ is the velocity and $u_e$ is the velocity at the edge of the boundary layer. The values of the nominal boundary-layer thickness $\delta$, displacement thickness $\delta_1$, and momentum thickness $\delta_2$, deduced from the velocity profiles are given in table 2. The corresponding mean pressure distributions (uncorrected for blockage) are presented in figure 3(*c*). A complete tabulation of the data has been given elsewhere (Güven, Patel & Farell 1975*b*).

The experiments for $Re = 1{\cdot}54 \times 10^5$ were made at two spanwise levels, one at a distance of 2·54 cm and the other at a distance of 0·32 cm above the mid-section, in order to assess the local influence of the roughness discontinuity provided, as explained in § 2·3, for the pressure taps. Upon comparison of the two sets of data presented in

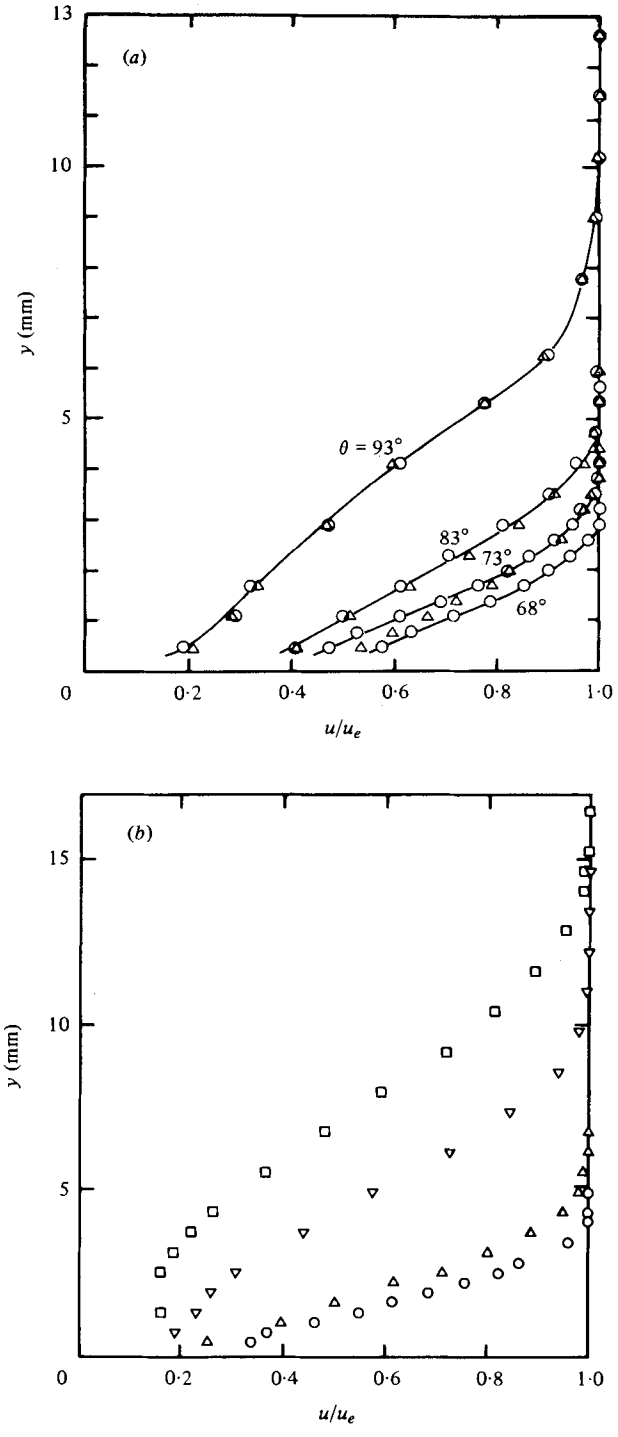


FIGURE 3 (*a*, *b*). For legend see p. 781.

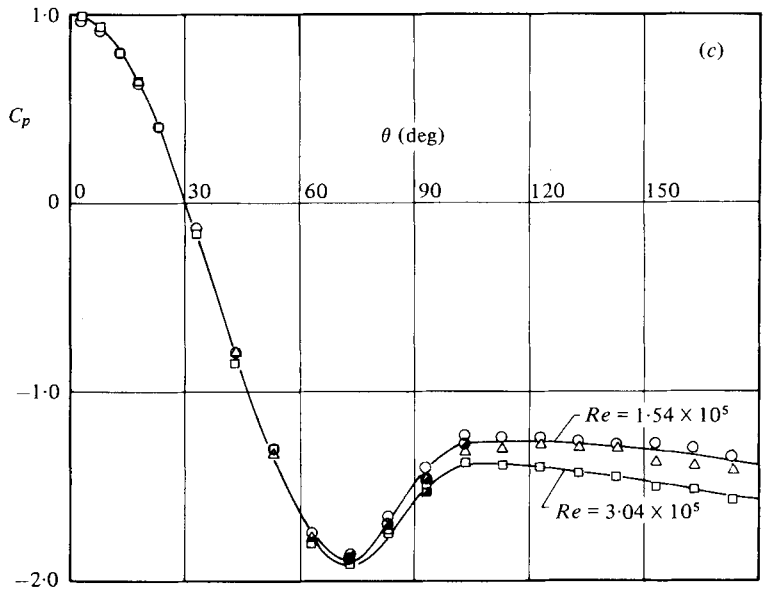


FIGURE 3. Boundary-layer velocity profiles and pressure distributions on the cylinder with the distributed roughness, $k/d = 2{\cdot}66 \times 10^{-3}$. (*a*) Velocity profiles, $Re = 1{\cdot}54 \times 10^5$: ○, traverse at 2·5 cm above midsection; △, traverse at 0·32 cm above midsection. (*b*) Velocity profiles, $Re = 3{\cdot}04 \times 10^5$: ○, $\theta = 73°$; △, $\theta = 83°$; ▽, $\theta = 93°$; □, $\theta = 98°$ (separated flow). (*c*) Pressure distributions. $Re = 1{\cdot}54 \times 10^5$: ○, △, different tests, obtained by computer; ◕, obtained manually. $Re = 3{\cdot}04 \times 10^5$: □, obtained by computer; ◪, obtained manually.

figure 3(*a*) and table 2, it appears that the effect of the discontinuity on the boundary-layer velocity profiles may be considered negligible in the context of the present study. The measurements for $Re = 3{\cdot}04 \times 10^5$ were made at a level 2·54 cm above the midsection.

## 4. Discussion

### 4.1. *Drag coefficient and important pressure distribution parameters*

The variation of the drag coefficient with Reynolds number and relative roughness for cylinders with distributed roughness is presented in figures 4(*a*, *b*). Here $k_d$ denotes the diameter of spherical roughness used by Szechenyi and Achenbach. Figure 4(*a*) shows the present results together with results from the smooth-cylinder tests of Roshko (1961) and Achenbach (1968), the tests of Achenbach (1971) with sandpaper roughness, and the uniform-stream tests of Batham (1973) with a smooth cylinder and with a cylinder roughened with sand particles. Also included are some results from Szechenyi (1975), Jones, Cincotta & Walker (1969) and Van Nunen, Persoon & Tijdeman (1974), although, as will be discussed below, a direct comparison of these $C_d$ results with the present ones and those of Achenbach and Roshko are made difficult by basic differences in the wind tunnels used. The results of Fage & Warsap (1929) are also shown, but only partially for clarity because Achenbach (1971) has already presented a comparison of his own results, which are shown here, with those of Fage & Warsap. It is useful to note that the foregoing $C_d$ results, other than those of Fage, Warsap and Jones *et al.*,

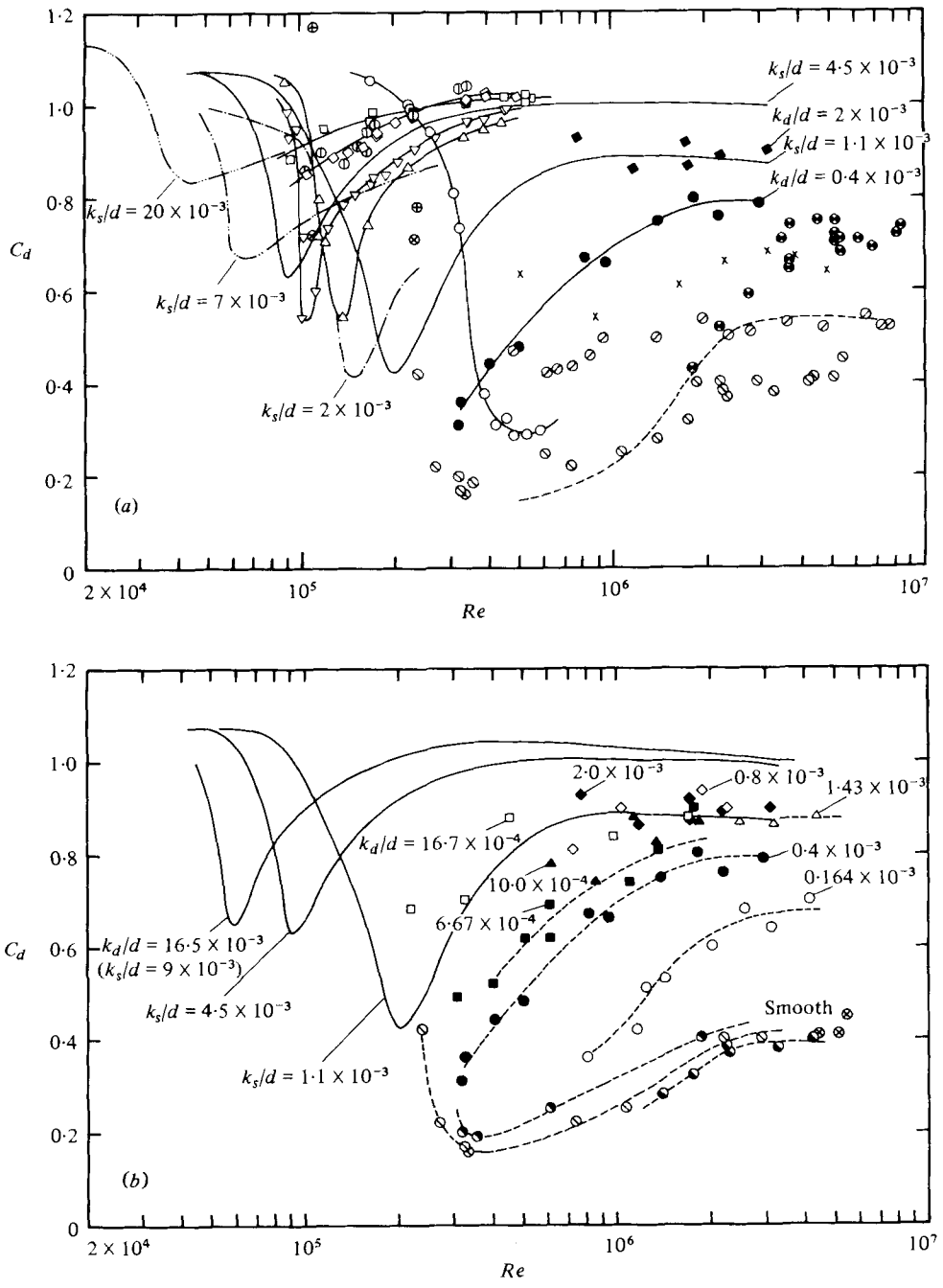


FIGURE 4. Drag coefficient. (*a*) Cylinders with distributed roughness. ——, Achenbach (1971), Fage & Warsap (1929): —·—, $k_s/d = 2 \times 10^{-3}$; —··—, $k_s/d = 7 \times 10^{-3}$; —···—, $k_s/d = 20 \times 10^{-3}$. Szechenyi (1975): ●, $k_d/d = 4 \times 10^{-4}$; ◆, $k_d/d = 2 \times 10^{-3}$. Present experiments: △, $k_s/d = 2{\cdot}5 \times 10^{-3}$; ▽, $k_s/d = 3{\cdot}11 \times 10^{-3}$; ⓘ, $k_s/d = 4{\cdot}18 \times 10^{-3}$ ($k/d = 3{\cdot}55 \times 10^{-3}$); ◇, $k_s/d = 6{\cdot}21 \times 10^{-3}$. ⊗, Batham (1973), $k/d = 2{\cdot}17 \times 10^{-3}$. Smooth cylinder results: ○, present: ×, Achenbach (1968); ⊕, Batham (1973); – – –, Jones *et al.* (1969); ⊛, Roshko (1961); ⊘, Szechenyi (1975); ⊘, Van Nunen *et al.* (1974). (*b*) Szechenyi (1975): ⊗, smooth cylinder in S2MA tunnel, $l/d = 4{\cdot}38$, $d/w = 0{\cdot}23$; ◔, ■, ▲, □, cylinder 1 in S3MA tunnel, $l/d = 9{\cdot}33$, $d/w = 0{\cdot}077$; ⊘, ●, ◇, ◆, cylinder 2 in S3MA tunnel, $l/d = 5{\cdot}6$, $d/w = 0{\cdot}128$; ◔, ○, △, cylinder 3 in S3MA tunnel, $l/d = 4{\cdot}0$, $d/w = 0{\cdot}179$. ——, Achenbach (1971).

have been obtained by integration of the pressure distributions and, in Achenbach's case, of the wall shear stresses as well. The $C_d$ values of Fage, Warsap and Jones *et al.* are based on direct drag measurements. Figure 4(*b*) is a re-presentation of all the results of Szechenyi (1975) identifying the different cylinders and the wind tunnels used. This information (which was not included in the original reference) as well as the numerical $C_d$ values necessary for preparation of the figure, were kindly made available to the authors by Szechenyi. For comparison, the results of Achenbach (1971) including those for the spherical roughness, are shown also in figure 4(*b*) (these results of Achenbach were not considered in Szechenyi 1974, 1975).

Figures 5, 6 and 7 show respectively the variations, with Reynolds number and relative roughness, of $C_{pb}$ and $C_{pm}$, $\theta_w$, and $C_{pb}-C_{pm}$. The $\theta_s$ curves of Achenbach (1971, figure 13) are included in figure 6 for comparison. For clarity, the present results corresponding to $k_s/d \times 10^3 = 3{\cdot}11$ and $4{\cdot}18$ have been excluded from figures 5 and 6. The results for these cases behave similarly (see discussion below) to the results shown for $C_d$ (figure 4*a*) and $C_{pb}-C_{pm}$ (figure 7). The values of $C_{pm}$, $C_{pb}$ and $\theta_w$ for Achenbach's cases have been evaluated from the detailed unpublished pressure distribution data kindly made available to the authors by Achenbach. (Corresponding results from Szechenyi 1975 could not be included in the figures as they are not available.) An examination of these parameters is important not only because they summarize the main characteristics of the pressure distributions but also because they shed light on the overall effects of surface roughness. Indeed it will be seen later that the pressure rise to separation, namely $C_{pb}-C_{pm}$, is closely related to the characteristics of the boundary layer at the location of the pressure minimum.

(*a*) *Drag coefficient.* In the discussion of the influence of roughness on the drag coefficient it is convenient first to consider the differences among the data from various sources to isolate major extraneous factors, and then examine the overall trends. It is well known that the flow past a cylinder is affected not only by the Reynolds number and the surface roughness but also by a multitude of other factors such as wind-tunnel blockage, length-to-diameter ratio and free-stream turbulence characteristics as well as model end conditions. Considering the nominally smooth cylinder data first, it is seen from figure 4(*a*) that there is a considerable variation over the entire range of Reynolds number among these data. It is believed that while this may be due in part to the fact that the 'smooth' surfaces act hydrodynamically rough at the larger Reynolds numbers, the primary reason is to be found in the basic differences in the wind tunnels and model configurations used in the experiments. The effective relative roughnesses, $k_s/d$, of Roshko's (1961), Achenbach's (1968), and Jones *et al.* (1969) cylinders, as estimated by each author, were $1{\cdot}0\times10^{-5}$, $1{\cdot}3\times10^{-5}$ and $0{\cdot}2\times10^{-5}$, respectively. This would appear to support the contention that the differences in $C_d$ values are at least in part due to differences in relative roughness, as Roshko (1970) tentatively inferred on the basis of these data and the data of Achenbach (1971), and as Jones *et al.* (1969) suggested earlier. However the differences are rather large, particularly if one considers the most recent data of Van Nunen *et al.* (1974) and Szechenyi (1975) for smooth cylinders in the trans-critical Reynolds-number range, also plotted in figure 4(*a*); Szechenyi's $C_d$ values are smaller than Roshko's by about 0·3, i.e., by more than 40 %. These differences in the drag coefficient are all the more surprising in view of the relatively close agreement of the corresponding values of the pressure difference $C_{pb}-C_{pm}$ shown in figure 7. Since, as indicated later on, this para-

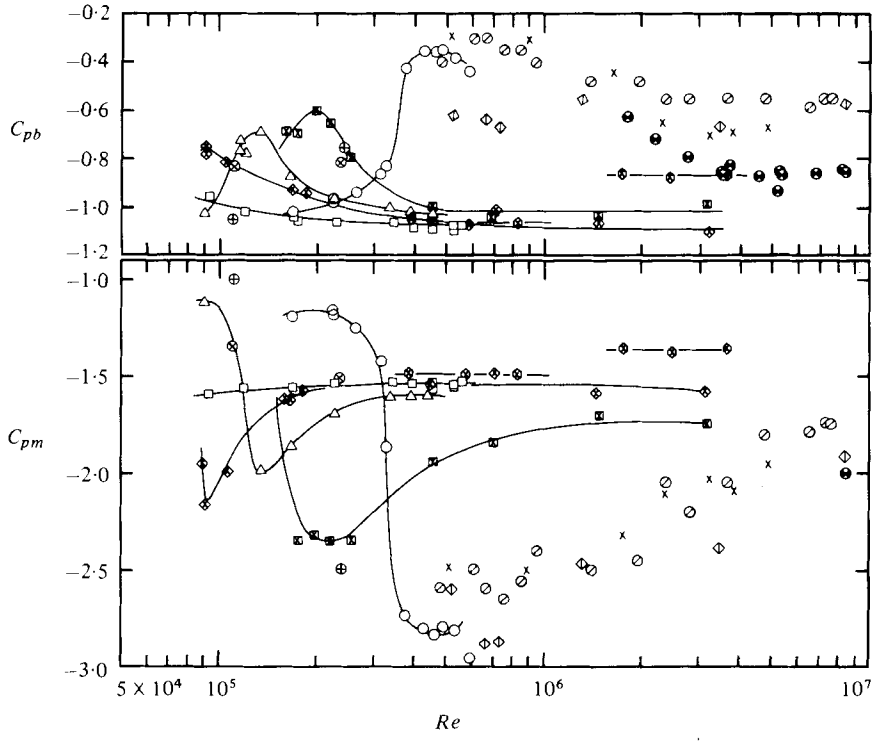


FIGURE 5. Base pressure coefficient and minimum pressure coefficient of cylinders with distributed roughness. Achenbach (1971): ⊠, $k_s/d = 1{\cdot}1 \times 10^{-3}$; ⊕, $k_s/d = 4{\cdot}5 \times 10^{-3}$; ⊗, $k_d/d = 16{\cdot}5 \times 10^{-3} (k_s/d = 9 \times 10^{-3})$. Present experiments: △, $k_s/d = 2{\cdot}5 \times 10^{-3}$; □, $k_s/d = 6{\cdot}21 \times 10^{-3}$; ⊗, Batham (1973), $k/d = 2{\cdot}17 \times 10^{-3}$. Smooth cylinder results: ○, present; ×, Achenbach (1968); ⊕, Batham (1973); ◇, Jones *et al.* (1969); ●, Roshko (1961); ⊘, Van Nunen *et al.* (1974).

meter is primarily a function of the surface roughness, the conclusion from figure 7 is that either the Reynolds numbers in these tests were not high enough for the smooth surfaces to act as hydrodynamically rough or that the effective roughnesses of the models in all given experiments were similar in magnitude. Furthermore, a detailed examination of the possible effects of the relatively minor differences in either free-stream turbulence intensity or in the length-to-diameter ratios of the models, which are better documented for rough surfaces, indicates that the observed differences in the $C_d$ values of the smooth cylinders could not be explained on the basis of these variables. A possible explanation is therefore the use of different means to correct the data for wind-tunnel blockage. The experiments of Roshko and Achenbach were performed in closed wind tunnels with solid walls and their data have been corrected for blockage using the method of Allen & Vincenti, for which experimental support is provided by the data of Farell *et al.* (1977). However, the other three studies utilized wind tunnels with slotted or perforated walls to compensate for blockage and it is possible that this may have resulted in an overcompensation. The relatively low values of $|C_{pb}|$ and $|C_{pm}|$ measured by Van Nunen *et al.* (figure 5) as well as the decrease (although not conclusive) in $C_d$ with increasing blockage ratio and decreasing $l/d$ shown by the smooth-cylinder data of Szechenyi in figure 4(*b*), an effect which is just the opposite of the one which would be expected in a solid-wall tunnel, would appear to

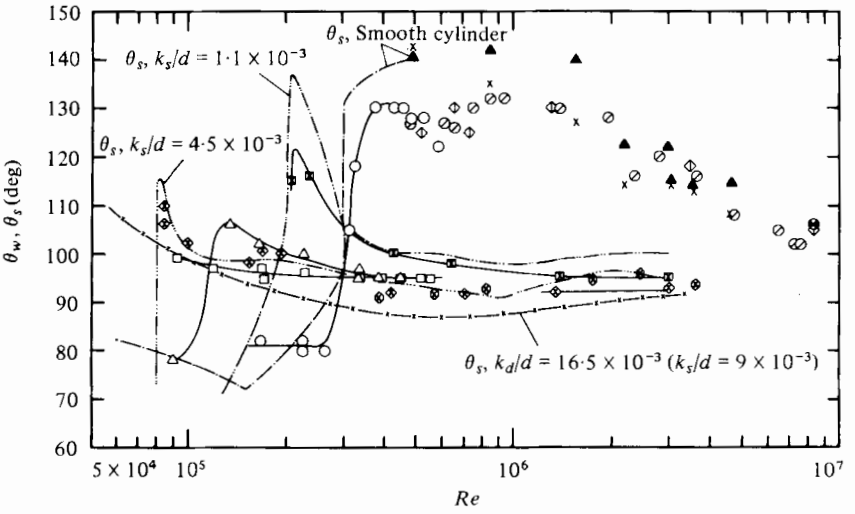


FIGURE 6. Variation of $\theta_w$ and $\theta_s$. $\theta_s$ results of Achenbach (1968, 1971): ▲, —·—, smooth cylinder; —··—, $k_s/d = 1{\cdot}1 \times 10^{-3}$; —···—, $k_s/d = 4{\cdot}5 \times 10^{-3}$; —×—, $k_d/d = 16{\cdot}5 \times 10^{-3}$ ($k_s/d = 9 \times 10^{-3}$). Other symbols denote the variation of $\theta_w$ and the notation for these is the same as in figure 5.

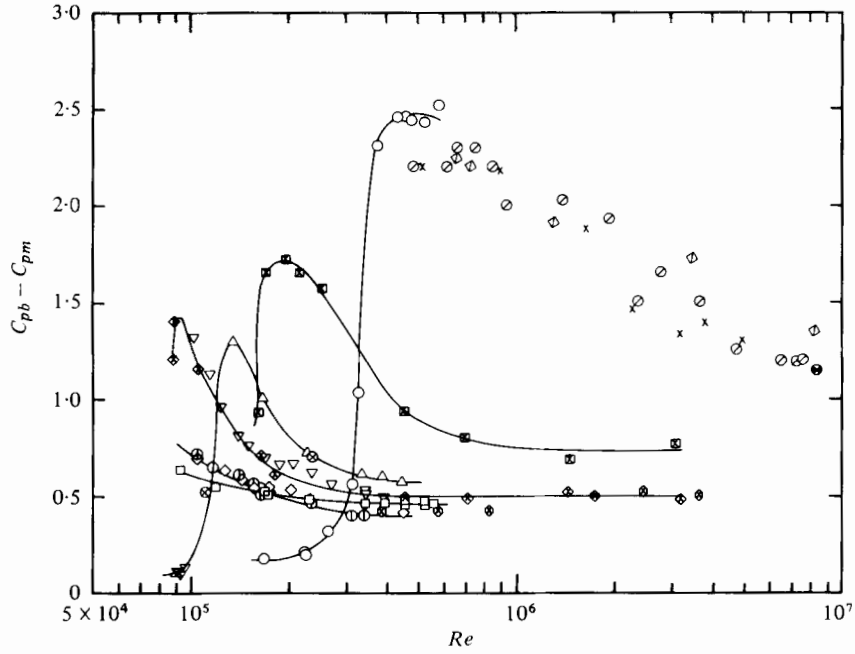


FIGURE 7. Variation of $C_{pb} - C_{pm}$. Cylinders with distributed roughness. Notation is as in figure 5. Present experiments: ▽, $k_s/d = 3{\cdot}11 \times 10^{-3}$; ⊙, $k_s/d = 4{\cdot}18 \times 10^{-3}$; ◇, $k_s/d = 4{\cdot}18 \times 10^{-3}$ ($k/d = 3{\cdot}55 \times 10^{-3}$).

support this view. Note that in the supercritical $Re$ range and for $l/d$ values between, say, 3 and 8, $C_d$ (corrected for blockage) appears to increase with decreasing $l/d$ in solid-wall wind tunnels (see Farell *et al.* 1977, figure 9 of Achenbach 1968, and the discussion below). (In connexion with slotted-wall wind-tunnel techniques, reference may be made to the *N.A.T.O. AGARD* Publication *CP*-174, March 1976.)

For cylinders with distributed roughness the main sources of earlier information are Fage & Warsap (1929), Achenbach (1971, 1977) and Szechenyi (1975). A comparison of the data of Fage & Warsap with those of Achenbach (1971) has been made already by Achenbach (1971, his figure 9) and a rather satisfactory agreement has been noted. Indeed, these results are in general agreement. It should be noted however that there are certain quantitive differences in the $C_d$ values obtained under similar roughness and Reynolds-number conditions. For example, at $Re = 2{\cdot}8 \times 10^5$, Fage & Warsap's $C_d$ values for both $k_s/d \times 10^3 = 4$ and 7 are significantly lower than Achenbach's value for $k_s/d \times 10^3 = 4{\cdot}5$. As the results have been corrected for blockage, the noted differences are most probably due to the differences in the length-to-diameter ratios ($l/d = 7{\cdot}88$ for Fage & Warsap's larger-diameter cylinder, $l/d = 3{\cdot}33$ in Achenbach's case) and in the end conditions of the test cylinders. Achenbach's cylinder completely spanned the test section, as in the present tests and all the others considered here, while Fage & Warsap's cylinder was suspended from a drag balance and had 3·2 mm gaps left between the ends of the 101·5 cm long test cylinder and the two extension cylinders used to fill the remaining portion of the 121·9 cm long span of the tunnel. (Because of the large surface roughness, the effect of the possible difference in upstream turbulence levels, 0·7 % in Achenbach's tests and unknown to the authors in Fage & Warsap's tests, is not expected to be significant. See also section 4.2.)

The differences in Achenbach's and Fage & Warsap's $C_d$ values may also be due to the different methods used in the measurement of $C_d$. While Fage & Warsap used direct drag measurements, Achenbach's values (as well as the other $C_d$ values considered here, except those of Jones *et al.* 1969) are based on integration of the pressure distributions at one section. We note incidentally that Jones *et al.* compared $C_d$ data obtained by direct integration of the pressure distributions with drag balance measurements (their figure 8). They found large discrepancies even in the trends of the curves relative to Reynolds number, and took the force balance measurements as accurate.

The present $C_d$ values are, as Achenbach's, larger than Fage & Warsap's in the supercritical $Re$ range, but a comparison on a quantitative basis, with regard to the effects of roughness, is difficult in view of the several aforementioned differences in the experimental arrangements and methods. It should be noted that comparison (figure 4*a*) of the $C_d$ result of Batham (1973) ($l/d = 6{\cdot}67$) for $k/d = 2{\cdot}17 \times 10^{-3}$ at $Re = 2{\cdot}35 \times 10^5$ with the present one ($l/d = 3{\cdot}08$) for $k/d = 2{\cdot}66 \times 10^{-3}$ (or even $k/d = 1{\cdot}59 \times 10^{-3}$) at the same $Re$ indicates that the present $C_d$ values are also larger than Batham's, which again may be due at least in part to the small $l/d$ of the present cylinder. The present results can be compared best (on a quantitative basis) with those of Achenbach (1971) as the experimental arrangements are most similar in these cases among all the studies considered. The present results are seen (figure 4*a*) to be in good general agreement with Achenbach's although there is some uncertainty concerning the values of $k_s/d$ assigned to the various roughnesses in the present experiments and there are some differences in the free-stream turbulence levels and

the length-to-diameter ratios of the cylinders. Together these results suggest that when the values of both $Re$ and $k_s/d$ are large enough, $C_d$ becomes nearly independent of both $Re$ and $k_s/d$ (the $Re$ range of the present setup is limited, particularly for small roughnesses). However, as shown by Achenbach's results for $k_s/d = 1{\cdot}1 \times 10^{-3}$, if the relative roughness is not large enough, $C_d$ continues to depend upon $k_s/d$ even at large Reynolds numbers and its value is smaller for smaller relative roughness. The recent experiments of Achenbach (1977) with pyramidal roughness also confirm these observations. The same trends are hinted at by the results of Fage & Warsap (1929), shown fully in Achenbach's (1971) figure 9, and partially in the present figure 4 (*a*), in spite of the quantitative differences discussed above. These observations are also supported, except for one data point for $k_d/d = 6{\cdot}67 \times 10^{-4}$ at $Re = 1{\cdot}77 \times 10^6$, by the data of Szechenyi (1975) shown fully in figure 4 (*b*). Considering the possible errors which Szechenyi (1975) has cautioned against, the scatter shown by the data, and also considering that the $C_d$ value corresponding to this single data point is slightly larger than the $C_d$ values corresponding to $k_d/d = 10^{-3}$ and to $k_d/d = 1{\cdot}67 \times 10^{-3}$ obtained with the same test cylinder ($d = 6$ cm) at about the same $Re$, it is very likely that the discrepancy shown by this single point is due to experimental error.

Finally, it should be noted that some scatter, in particular in the case of $k_s/d = 4{\cdot}18 \times 10^{-3}$ ($k/d = 2{\cdot}66 \times 10^{-3}$), and non-monotonicity are shown by the present data. The scatter may be taken as a measure of the possible experimental errors; the non-monotonicity is believed to be due partly to the different textures, noted earlier, of the two coarsest papers used, and partly to experimental errors.

(*b*) *Pressure distributions.* The foregoing would indicate that observations based on the $C_d$ results alone may be misleading in certain cases and an examination of the detailed pressure distributions is necessary. As seen from figure 5, both $C_{pb}$ and $C_{pm}$ obtained with sandpaper roughness show well defined trends with Reynolds number and relative roughness, as did the drag coefficient. Examination of the curves for $k_s/d \times 10^3 = 2{\cdot}50$ shows that $|C_{pb}|$ becomes a minimum and $|C_{pm}|$ a maximum at the same Reynolds number for which the corresponding drag coefficient curve in figure 4 (*a*) indicates a minimum value of $C_d$. As the Reynolds number increases beyond this value, $|C_{pm}|$ decreases while $|C_{pb}|$ and $C_d$ increase, until all attain nearly constant values asymptotically at some large Reynolds number.

The results for the large spherical roughness tested by Achenbach (1971) ($k_d/d = 16{\cdot}5 \times 10^{-3}$; $k_s/d = 9 \times 10^{-3}$ as estimated by Achenbach) show however a peculiar (and heretofore unnoticed) behaviour beyond $Re \simeq 10^6$. The data appear to show a jump in the values of both $C_{pb}$ and $C_{pm}$ beyond this $Re$. The values are significantly different in this $Re$ range from those for the large sandpaper roughnesses as well. The different behaviour is evidently due to the very large spherical roughness used, although the reasons are not entirely clear. It may be useful to recall that coherent vortex shedding was observed by Szechenyi (1975, his figure 6) to be destroyed by large spherical roughnesses beyond a roughness Reynolds number, $V_0 k_d/\nu$ of about 9200. The drop in the value of $|C_{pb}|$ seen in figure 5 for Achenbach's spherical roughness is consistent with an increased three-dimensionality of the unsteady flow and spanwise irregularity of the separation line, and thus suggests that the two different observations noted above may be connected.

The variation of the angle $\theta_w$ with Reynolds number and relative roughness is depicted in figure 6. It was noted earlier that $\theta_w$ may be regarded as a rough indicator

of the location of separation. This is illustrated by the correlation between $\theta_w$ and $\theta_s$, the actual mean location of separation, depicted in this figure on the basis of Achenbach's (1968, 1971) data. Comparison of figures 5 and 6 shows that, as $\theta_w$ decreases in the supercritical Reynolds-number range, i.e., as the separation point moves upstream, $|C_{pb}|$ increases and $|C_{pm}|$ decreases. It can also be seen from figure 6 that $\theta_w$ shows the same transitional changes with Reynolds number as do $C_d$, $C_{pm}$ and $C_{pb}$. However, Achenbach's data for the large spherical roughness show a difference from the other data in the behaviour of $\theta_w$ and $\theta_s$, $\theta_s$ being generally smaller than $\theta_w$ in this case whereas for the other cases $\theta_s$ is generally larger than $\theta_w$. The reasons for this are not entirely clear. It should be recalled however that Achenbach (1971) had cautioned about the possible qualitative nature of the shear-stress data obtained for the large spherical roughness as the shear-stress probe was not calibrated in this case. It is useful to note that the recent data of Achenbach (1977) for pyramidal roughnesses show that $\theta_s$ (inferred from the curves of local heat-transfer coefficient) is consistently larger than $\theta_w$ in the supercritical $Re$ range for all the roughnesses tested. In particular, the values of $\theta_w$ at $Re = 4{\cdot}6 \times 10^6$ inferred from figure 9 of Achenbach (1977) range between 98° and 92° while corresponding $\theta_s$ inferred from figure 17 of the same paper range between 110° and 105°, both $\theta_s$ and $\theta_w$ decreasing with increasing roughness. The relative heights $h_{\text{eff}}/d$ of the pyramidal roughness used were $7{\cdot}3 \times 10^{-4}$, $3 \times 10^{-3}$, and $6 \times 10^{-3}$.

The overall effect of surface roughness on the pressure distributions is best seen in figure 7. In the supercritical Reynolds-number range, $C_{pb} - C_{pm}$ decreases with increasing $Re$ for a given relative roughness and decreases with increasing relative roughness for a given Reynolds number. Furthermore, the incremental changes in $C_{pb} - C_{pm}$ decrease with increasing roughness. The present boundary-layer measurements and related analysis (§ 4.2) suggest that the pressure difference $C_{pb} - C_{pm}$ is closely related to the characteristics of the boundary layer prior to separation and therefore its strong dependence on relative roughness is not surprising. The quantity $C_{pb} - C_{pm}$ is also important because it is quite insensitive to effects of tunnel blockage and $l/d$ (see Farell *et al.* 1977) and even free-end effects (see Farell, *et al.* 1976, for a detailed comparison between cylinder and cooling-tower results). The good agreement shown in figure 7 by the nominally smooth cylinder results of Achenbach, Roshko, Van Nunen *et al.* and Jones *et al.*, despite the large differences in the corresponding $C_d$, $C_{pb}$ and $C_{pm}$ values noted earlier, further confirms this observation. It may also be seen from figure 7 that even the spherical-roughness data which was noted to display a jump (of about 0·2) in the values of $C_{pb}$ and $C_{pm}$ beyond $Re \simeq 10^6$ show a smaller jump (of about 0·07) in terms of $C_{pb} - C_{pm}$.

(*c*) *Large-Reynolds-number behaviour.* From the various data on the drag coefficient and the pressure-distribution parameters shown in figures 4–7, there are certain general trends which can be deduced concerning the influence of Reynolds number and surface roughness in spite of the several additional factors, such as the determination of the effective roughness, tunnel blockage, freestream turbulence, and length-to-diameter ratios of the models, which undoubtedly influence the results. In particular, it is observed that for each relative roughness there is an upper value of Reynolds number beyond which the various gross parameters become independent of Reynolds number and attain nearly constant values. Furthermore, these asymptotic, $Re$-independent values appear to depend upon the relative roughness parameter $k_s/d$, and become

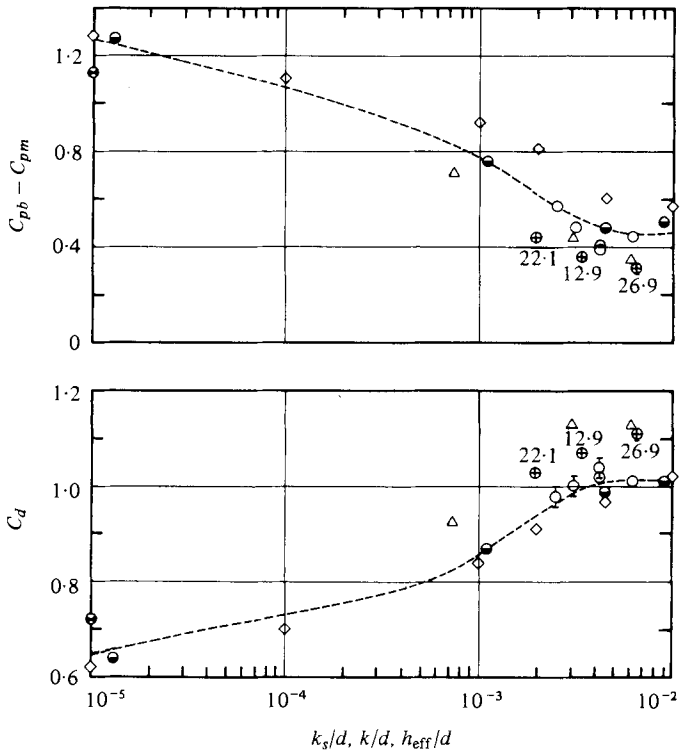


FIGURE 8. Variation of $C_{pb} - C_{pm}$ and $C_d$ with $k_s/d$ ($k/d$ for ribs, $h_{\text{eff}}/d$ for pyramidal roughness) at large $Re$. (The value of $s/k$ is shown next to each point for cylinders with ribs.) Cylinders with distributed roughness: ○, ⊖, present experiments; ⊖, Roshko (1961); ◒, Achenbach (1968, 1971). △, cylinders with pyramidal roughness (Achenbach 1977); ◇, calculations (Güven *et al.* 1977); ⊕, cylinders with ribs (Güven *et al.* 1975*a*).

independent of it for sufficiently large $k_s/d$. The data shown in figures 4 and 7 have been used to estimate the $Re$-independent values of $C_d$ and $C_{pb} - C_{pm}$ and these are plotted as functions of $k_s/d$ in figure 8. The dotted lines have been inserted simply to indicate the overall trends for sandpaper roughness. It should be emphasized that these estimates contain the uncertainties associated with the limited Reynolds-number range of the present experiments as well as the values of $k_s/d$ assigned to the various sandpapers. (Error estimates are indicated in the figure.) In some instances (e.g., $k_s/d \times 10^2 = 2{\cdot}50$ and $3{\cdot}11$) $C_{pm}$ and $\theta_w$ appear to approach the asymptotic values faster than $C_d$ and $C_{pb}$ and consequently the error in the estimation of the latter is somewhat larger (about 0·03 in magnitude). Although the 'smooth' cylinder data of Roshko and Achenbach cannot strictly be considered $Re$ independent, they have been included since these tests were performed at quite high Reynolds numbers ($8{\cdot}4 \times 10^6$ and $5 \times 10^6$, respectively) and the data in the original references indicate very little further change, if any, in $C_d$ with increasing $Re$. Also included in figure 8 are data from Achenbach (1977) obtained with pyramidal roughnesses, from Güven (1975) for cylinders with rib roughnesses ($s$ being the circumferential spacing and $k$ the height of the ribs) as well as the results of the calculations of Güven *et al.* (1977) for sandpaper roughness. (A similar figure, without the rib-roughness data and the recent pyramidal-roughness

data of Achenbach was presented earlier in Güven *et al.* 1977, but the data could not be discussed in detail there.)

*Although there is some* scatter in the data, figure 8 indicates that surface roughness has a significant direct influence on the drag coefficient and the pressure distribution parameters even at large Reynolds numbers where the mean flow achieves independence from Reynolds number. It is seen that, as the relative roughness increases, $C_{pb}-C_{pm}$, which is about 1·2 for nominally smooth cylinders, decreases and obtains a value around 0·45 for large roughnesses. The drag coefficient $C_d$ also increases with increasing roughness and reaches a nearly constant value, of the order of 1·0, for large relative roughnesses. Overall, the major changes with $k_s/d$ appear to occur up to about $k_s/d \simeq 3\times10^{-3}$. Figure 6 and the corresponding pressure distributions further suggest that $\theta_w$ decreases with increasing roughness, from about 105 degrees for 'smooth' cylinders to about 95 degrees for values of $k_s/d$ greater than about $3\times10^{-3}$. The correspondence between $\theta_w$ and the mean location of separation, $\theta_s$, shown by the data of Achenbach in figure 7 would indicate that $\theta_s$ is roughly 5 degrees greater than the $\theta_w$ values quoted above. Thus, the asymptotic location of separation at large Reynolds numbers and with large relative roughness would appear to be 100 degrees rather than 90 degrees as conjectured by Roshko (1970). The detailed pressure distributions examined during the course of the study indicate further that the location of the pressure minimum, $\theta_m$, remains substantially unaffected by roughness at large Reynolds numbers and occurs in the range 72–76 degrees. The foregoing quantitative observations apply to sandpaper-type roughness and for relative roughnesses less than $k_s/d = 10^{-2}$ as data (or a theory) for larger relative roughness are not available. It should be noted that the data for cylinders with ribs or with pyramidal roughness as well as with spherical roughness show similar trends qualitatively.

It is interesting to compare the correlations depicted in figure 8 with the somewhat different correlation presented by Szechenyi (1975) in his figure 3, where he plotted $C_d$ as a function of the roughness Reynolds number $V_0 k_d/\nu$ using only his data and those of Fage & Warsap. From this he concluded that, 'within broad limits of experimental error' and for $V_0 k_d/\nu > 200$, $C_d$ is independent of $Re$ (the cylinder Reynolds number) but depends upon the roughness Reynolds number, and eventually becomes independent of it for $V_0 k_d/\nu > 1000$ and attains a nearly constant value of 0·9. There are several important similarities and differences between these observations and figure 8 which need to be explored.

Szechenyi's conclusion that, for sufficiently large values of $V_0 k_d/\nu$ (which implies large values of $Re$ as well as $k_s/d$, the parameters used here), $C_d$ approaches a constant value of about 0·9 is in substantial agreement with the conclusion drawn from the present correlation in figure 8, which indicates an asymptotic value of $C_d \doteqdot 1{\cdot}0$. (Note that Szechenyi's $C_d$ values may require a correction for wind tunnel blockage, as discussed in § 4.1 (*a*).) The asymptotic behaviour at large Reynolds numbers can be attributed to the expectation that at large $Re$ the boundary layer on the cylinder is turbulent over most of the surface (i.e., transition occurs early) and that the surface acts as if it were fully-rough in the sense of Nikuradse, making the boundary layer flow independent of viscosity. (An explanation of the 'asymptotic' behaviour for large $k_s/d$, but not larger than $10^{-2}$, indicated by the data discussed in the preceding paragraphs is not so obvious and reference should be made to the calculations of Güven *et al* (1977), the results of which are reproduced in the present figure 8. The case of

unusually large roughness, $k_s/d > 0{\cdot}01$, is not discussed here.) If the present data and those of Achenbach (1971) and others are included in Szechenyi's correlation, the agreement is surprisingly good although the 'broad limits of experimental error' become broader over the entire range of roughness Reynolds numbers of interest. This would suggest that another parameter is needed to explain the scatter, which is not insignificant in magnitude. Although there are several candidates for this, including free-stream turbulence, length-to-diameter ratio and so on, it is argued here that the two basic parameters have already been identified, namely $Re$ and $k_s/d$, and that the asymptotic $Re$ independent state is dependent on $k_s/d$. Szechenyi's roughness Reynolds number is no more than the product of these two parameters. Their use separately, as recommended here, re-establishes the cylinder Reynolds number as the primary measure of the overall influence of viscosity and explains the scatter in the correlation of Szechenyi.

### 4.2. *Boundary-layer characteristics*

Although it is well known that the changes in the pressure distribution and drag coefficient of circular cylinders with Reynolds number and surface roughness are related to changes in the behaviour of the boundary layer, there is little quantitative information available on the boundary-layer properties in the various flow regimes. The parameters which are of primary interest are the location of transition $\theta_t$, the extent of the separation bubble when one is present, the location of the eventual separation $\theta_s$, and boundary-layer properties such as velocity profiles, integral thicknesses, shape parameter and local friction coefficient. Unfortunately, the documentation of these is quite difficult since the boundary layer is usually very thin and the overall flow is generally unsteady. This is well evidenced by the lack of such information despite the large number of experimental investigations on cylinders over the past several decades. Nevertheless, as the measurements of Achenbach (1971, 1977) indicate, some information is available on the locations of transition and separation and their movements with Reynolds number and surface roughness. These show that four flow régimes, each characterized by a special boundary-layer behaviour, can be identified, namely subcritical (purely laminar separation), critical (laminar separation followed by turbulent reattachment and eventual turbulent separation), supercritical (transition occurring ahead of separation and moving upstream) and transcritical (transition located sufficiently close to the forward stagnation line to render the flow nearly independent of Reynolds number). (The notation here follows that of Achenbach 1971 except possible for the beginning of the supercritical range.) The present boundary-layer measurements and the associated analytic study were undertaken largely to complement this existing information and establish a quantitative connexion between the boundary layer and the observed variation of the drag coefficient and pressure-distribution parameters with surface roughness and Reynolds number, discussed in the previous sections.

Figure 9 shows the velocity profiles across the boundary layer in the neighbourhood of the location of the pressure minimum $\theta_m$ measured at two cylinder Reynolds numbers with the distributed roughness $k/d = 2{\cdot}66 \times 10^{-3}$ ($k_s/d = 4{\cdot}18 \times 10^{-3}$). Also shown there is the velocity distribution measured by Patel (1968) at a somewhat higher Reynolds number on a smooth cylinder fitted with trip wires at $\theta = \pm 45°$. The table in the figure legend lists the non-dimensional boundary-layer thickness $\delta/d$ and momen-

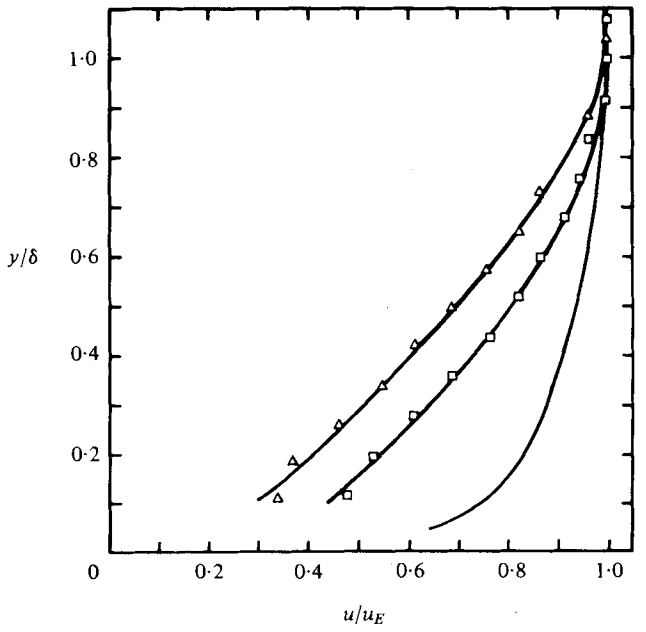


FIGURE 9. Effect of distributed surface roughness and Reynolds number on the boundary-layer velocity profile at or near the location of the minimum pressure.

| | $k/d \times 10^3$ | $Re \times 10^{-5}$ | $\delta_2/d$ near $\theta_m$ | $\delta/d$ near $\theta_m$ | $\theta_w$ | $C_{pb}-C_{pm}$ | $C_{pm}$ |
|---|---|---|---|---|---|---|---|
| —△—, Present study | 2·66 | 3·04 | $2{\cdot}52 \times 10^{-3}$ | 0·0146 | 95° | 0·46 | −1·91 |
| —□—, Present study | 2·66 | 1·54 | $1{\cdot}95 \times 10^{-3}$ | 0·0141 | 98° | 0·59 | −1·90 |
| ———, Patel (1968) | Smooth cylinder with trip wires at $\theta = \pm 45°$ | 5·01 | $1{\cdot}3 \times 10^{-3}$ | 0·0160 | 102° | 1·20 | −2·00 |

tum thickness $\delta_2/d$ at $\theta_m$, the minimum pressure coefficient $C_{pm}$ and the pressure rise parameter $C_{pb}-C_{pm}$. Perhaps the most interesting observation from the table is the close correlation between the momentum deficit of the boundary layer at $\theta_m$ and the pressure rise to separation and the angle at which separation occurs. It is clear that the boundary layer with the largest momentum deficit separates earlier and sustains the smallest pressure rise. (Note that one could equally well use the displacement thickness of the boundary layer or the local shear stress at $\theta_m$ in place of the momentum thickness in order to characterize the state of the boundary layer there.) This correlation is particularly noteworthy in view of the fact that the physical thickness of the boundary layer as well as the minimum pressure coefficient are virtually the same in all three cases. Although the Reynolds number, the surface roughness, and the location of transition all influence the state of the boundary layer at $\theta_m$, figure 9 suggests the possibility of relating the location of separation ($\theta_s$ or $\theta_w$) and the pressure rise to separation ($C_{pb}-C_{pm}$) to the properties of the boundary layer at $\theta_m$, the latter being inferred from usual boundary-layer calculation procedures. The present boundary-layer measurements have therefore been used in conjunction with simple analytical models to explore these possibilities.

The observation that the distance to separation ($\theta_w - \theta_m$) and the pressure rise to separation ($C_{pb} - C_{pm}$) should be correlated with the boundary-layer characteristics at the reference point $\theta_m$ is not new to those familiar with boundary-layer behaviour. However, as noted earlier, the authors are not aware of a systematic study of boundary-layer development on circular cylinders, particularly with surface roughness where the flow over most of the surface is turbulent. An attempt was therefore made to adopt simple but well proven boundary-layer calculation procedures, assess their validity by comparison with available measurements and then use them to explain the observed dependence of some of the gross pressure-distribution parameters on Reynolds number and surface roughness.

Insofar as the boundary-layer calculations are concerned, it was assumed that the pressure distribution on the cylinder is known and that the location of transition can be determined *a priori*. In fact, the results of Feindt (1957) and Hall & Gibbings (1972) were used to deduce a criterion for transition which relates the displacement-thickness Reynolds number at transition to the free-stream turbulence intensity and relative surface roughness (see Güven 1975). The momentum integral equation was used to calculate the laminar boundary layer from $\theta = 0$ to $\theta_t$, using an empirical relation (Güven 1975) to account for the effect of roughness on the wall shear, and assuming a parabolic velocity distribution in the boundary layer. For small relative roughnesses, the method of Thwaites was used as discussed in Rosenhead (1963). The subsequent turbulent boundary-layer development was calculated by the entrainment method of Head (1958), modified to include the friction-coefficient correlation of Dvorak (1969). The calculations are quite simple and since the procedures are well documented in original publications as well as Güven (1975) and Güven *et al* (1977), they are not discussed here. However, it is of interest to highlight the major conclusions drawn from the many calculations that were performed over a range of values of $Re$ and $k_s/d$.

It was observed that the boundary-layer calculations did not predict separation when the measured pressure distribution was used. However, if the pressure distribution in the neighbourhood of $\theta_w$ is modified by extrapolation from the largest adverse pressure gradient, as shown in figure 10, then separation is predicted some distance downstream of $\theta_w$. This observation is not new and simply indicates the breakdown of first-order boundary-layer theory in the vicinity of separation and the importance of the interaction between the viscous and the inviscid flow as well as the unsteadiness associated with the separation and the wake. Nevertheless, boundary-layer calculations on the basis of consistently extrapolated pressure distributions lead to several useful results. First, calculations performed for the smooth cylinder experiments of Achenbach (1968) at $Re = 4{\cdot}65 \times 10^6$ and Roshko (1961) at $Re = 8{\cdot}4 \times 10^6$ indicated separation at 115 and 116 degrees, respectively, in substantial agreement with the observed separation positions: $\theta_s = 112$ degrees in the first case (according to figure 10 of Achenbach 1968) and $\theta_w = 106$ degrees for Roshko's pressure distribution. (It may be noted here that asymmetries in the flow, of the order of a few degrees in the position of separation, were observed by Achenbach (private communication), and that the values of $\theta_s$ shown in figure 13 of Achenbach (1971), which are averages of the values measured on both sides of the cylinder, are smaller than the values inferred from the shear-stress distributions in figures 10 and 11 of the same paper.) These and other calculations at such high Reynolds numbers also indicated a marked insensitivity of the separation position to the location of transition, which moves upstream with

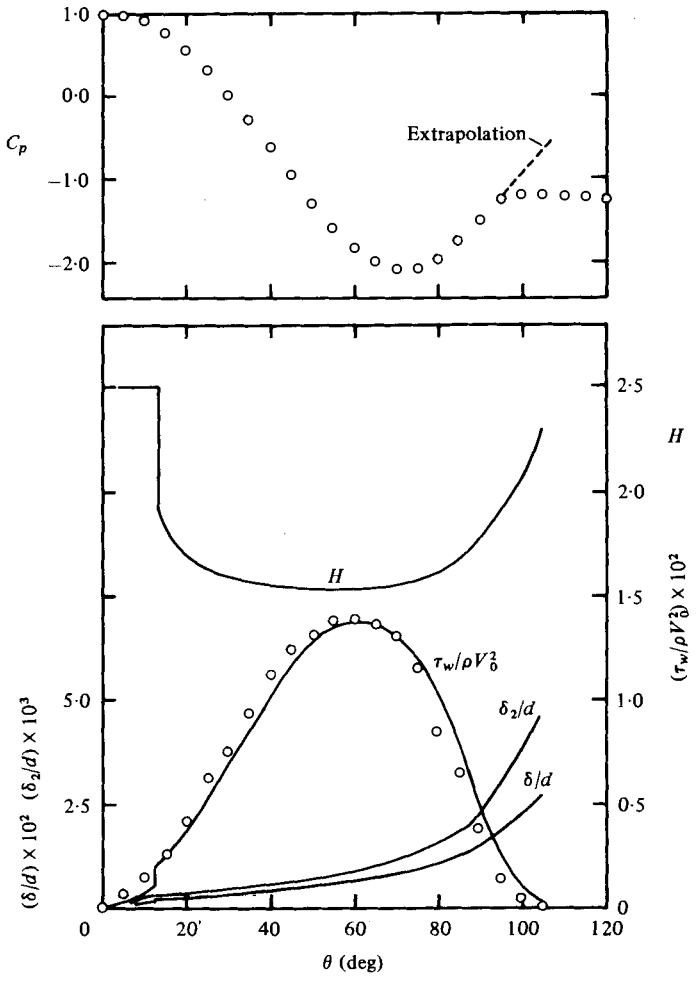


FIGURE 10. Boundary-layer development on a cylinder with distributed roughness. ○, experimental measurements of Achenbach (1971), $k_s/d = 1{\cdot}1 \times 10^{-3}$, $Re = 3 \times 10^6$, free-stream turbulence intensity 0·7 %. ——, present calculations.

increasing Reynolds number in the supercritical range. (The $\theta_t$ data of Achenbach 1968 and 1971 are consistent with these findings.) Secondly, calculations with small surface roughness were successful in predicting not only the location of separation but also some of the detailed features of the boundary layer. This is shown in figure 10, which corresponds to the measurements of Achenbach (1971) at $Re = 3 \times 10^6$ and $k_s/d = 1{\cdot}1 \times 10^{-3}$. Note that the calculations indicate transition at $\theta = 12$ degrees, separation at $\theta = 105$ degrees (with the extrapolated pressure distribution) and give good overall agreement with the measured wall shear stress distribution. Finally, similar comparisons made with surface roughness greater than about $2{\cdot}5 \times 10^{-3}$, including all the present experiments as well as the large roughness experiment of Achenbach ($k_s/d = 4{\cdot}5 \times 10^{-3}$), showed a marked disagreement with the available boundary-layer data, particularly downstream of the location of minimum pressure coefficient. This is undoubtedly due to the failure of the several gross assumptions

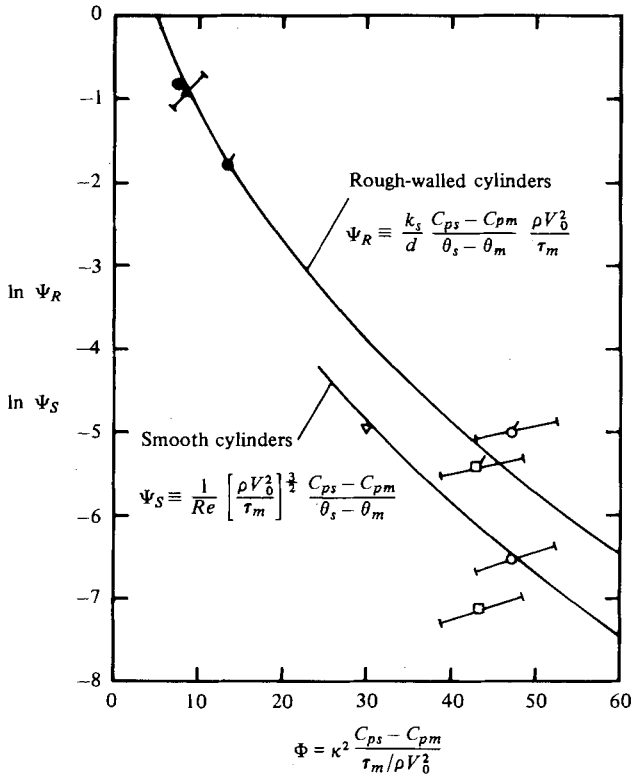


FIGURE 11. Boundary-layer separation criterion for smooth and rough-walled circular cylinders. ——, theory; △, present experiment, $k_s/d = 4{\cdot}18 \times 10^{-3}$ $(k/d = 2{\cdot}66 \times 10^{-3})$, $Re = 3 \times 10^5$; ●, Achenbach (1971), $k_s/d = 4{\cdot}5 \times 10^{-3}$, $Re = 3 \times 10^6$; ◐, Achenbach (1971), $k_s/d = 1{\cdot}1 \times 10^{-3}$, $Re = 3 \times 10^6$; ○, Achenbach (1968), smooth cylinder, $Re = 4{\cdot}56 \times 10^6$; □, Roshko (1961), smooth cylinder, $Re = 8{\cdot}4 \times 10^6$; ◌, Achenbach's smooth-cylinder result plotted with the assumption of fully-rough flow with $k_s/d = 1{\cdot}3 \times 10^{-5}$; ◻, Roshko's smooth-cylinder result plotted with the assumption of fully-rough flow with $k_s/d = 1{\cdot}0 \times 10^{-5}$; ▽, Patel (1968), smooth cylinder, tripped at $\theta = \mp 45°$, $Re = 15 \times 0^5$.

made in the method for the calculation of the turbulent boundary layer. Nevertheless, the calculations could be used to assess the state of the boundary layer at the pressure minimum with some confidence. In view of this, a separate analysis was attempted for the boundary-layer development in the region of the pressure rise to separation, i.e., $\theta_m < \theta < \theta_s$.

To describe the boundary-layer development between $\theta_m$ and $\theta_s$, the two-layer model of Stratford (1959) and its improvement by Townsend (1962) was generalized to include the influence of surface roughness. This involves the replacement of the smooth-surface law of the wall by the hydrodynamically-rough surface law of the wall to describe the velocity distribution in the constant-stress inner layer. The analysis parallels that of Townsend and is outlined in Güven *et al.* (1977) and described in detail by Güven (1975).

The theoretical curves resulting from this analysis are plotted in figure 11 where $C_{ps}$ is the pressure coefficient at $\theta_s$, $\tau_m$ is the wall shear stress at $\theta_m$ and $\kappa = 0{\cdot}41$. Comparison of these with experimental data is hampered somewhat by the lack of direct informa-

tion on the wall shear stress at $\theta_m$. Nevertheless, six experiments were identified in which this quantity could be estimated with some certainty. The values of the relevant parameters used to plot the points in figure 11 are given in table 3. With the exception of Roshko's experiment, the pressure distributions used were not corrected for blockage since, as noted earlier, the pressure rise is fairly insensitive to blockages less than about 15 %. The values of the wall shear stress $\tau_m/\rho V_0^2$ associated with the smooth-cylinder experiments of Roshko (1961) and Achenbach (1968) were calculated by the detailed boundary-layer computation procedure discussed above. Experimental shear stress values are available for the case of Achenbach (1968), but these were found to be in error (see Güven 1975) which was probably because the shear-stress probe was not calibrated for turbulent flow during the smooth cylinder experiments, as Achenbach himself has noted. In the case of the rough-walled cylinders of Achenbach (1971), the wall shear stress was obtained from his data (figures 10 and 11 of his paper) which were found to be in excellent agreement with the present boundary-layer calculations (see figure 10). For the smooth-cylinder data of Patel (1968), the wall shear stress was deduced from the measured velocity profile at $\theta_m$ and the well known smooth-surface skin-friction formula of Ludwieg and Tillmann. Finally, the value of $\tau_m/\rho V_0^2$ for the present experiment with $k_s/d = 4{\cdot}18 \times 10^{-3}$ was estimated from the measured momentum-thickness development using the momentum integral equation. (Note that the lack of velocity profile data in the neighbourhood of the wall and the uncertainty associated with the effective location of the surface precluded the use of the measured velocity profiles to determine the wall shear stress.)

Since the previous detailed boundary-layer calculations for the smooth cylinder experiments of Roshko and Achenbach had indicated that the boundary layer at $\theta_m$ was turbulent but not fully rough, these data are compared with the smooth-wall expression in figure 11. On the other hand, as discussed in § 4.1 (*c*) these experiments were performed at Reynolds numbers which are sufficiently high for the flow to become nearly independent of Reynolds number. Since further increase in Reynolds number is not expected to produce substantial changes in either the pressure distribution or the values of $\tau_m/\rho V_0^2$, although the boundary layer in the region $\theta_m < \theta < \theta_s$ would approach a fully-rough condition, the data are compared also with the rough-wall expression using the effective surface roughness noted earlier and listed in table 3.

In spite of the various assumptions made in the analysis which need to be investigated in detail and the unavoidable uncertainties associated with the use of experimental data to estimate the various quantities appearing therein, in particular the appropriate value of $\tau_m/\rho V_0^2$ for the present experiments, figure 11 shows that there is good general agreement between theory and experiments. Possible shifts in the experimental points due to the uncertainties have been estimated and are not so large as to affect the general conclusion. (Shifts due to a $\pm 10$ % uncertainty in $\tau_m/\rho V_0^2$, $\pm 20$ % in the case of the present experiment, are indicated in the figure.) The theory therefore supports the observation made from figure 9 and the table in the legend, that the pressure rise to separation, $C_{ps} - C_{pm}$ (which is essentially equal to $C_{pb} - C_{pm}$), on a circular cylinder is primarily a function of the state of the boundary layer at the pressure minimum, which, in turn, depends upon the values of $k_s/d$, $Re$ and $\tau_m/\rho V_0^2$. Note also that the term $(C_{ps} - C_{pm})/(\theta_s - \theta_m)$ (which is of the order of 1 to 2) varies little in comparison with $k_s/d$ over the wide range of roughness conditions examined here. Consequently, the value of $\ln \Psi_R$, and therefore $\Phi$, is determined

| Source | Symbol in figure 11 | $k_s/d \times 10^5$ | $Re \times 10^{-5}$ | $\tau_m/\rho V_0^2 \times 10^3$ | $\theta_m$ (deg) | $\theta_s$ (deg) | $C_{pm}$ | $C_{ps}$ | $C_{ps}-C_{pm}$ |
|---|---|---|---|---|---|---|---|---|---|
| Roshko 1961 | □ □ | 1·0 | 84 | 4·5 | 75 | 108 | −2·00 | −0·85 | 1·15 |
| Achenbach 1968 | ○ ○ | 1·3 | 46·5 | 5·0 | 82 | 115 | −2·25 | −0·85 | 1·40 |
| Patel 1968 | ▽ | — | 5 | 6·75 | 75 | 110 | −2·00 | −0·80 | 1·20 |
| Achenbach 1971 | ● | 110 | 30 | 11·5 | 75 | 105 | −2·10 | −1·20 | 0·90 |
| Achenbach 1971 | ● | 450 | 30 | 13·6 | 75 | 100 | −1·95 | −1·35 | 0·60 |
| Present Study | △ | 418 | 3·04 | 11·2 | 73 | 103 | −1·91 | −1·35 | 0·56 |

TABLE 3. Values used in the calculation of the data points of figure 11.

primarily by $k_s/d$ and $\tau_m/\rho V_0^2$. Since $\tau_m/\rho V_0^2$ is itself dependent on the relative roughness and becomes independent of $Re$ at sufficiently large $Re$, the theory also explains the dependence of $C_{ps}-C_{pm}$ on the value of $k_s/d$ at sufficiently large Reynolds number, as was implied by the correlation shown in figure 8. Furthermore, it is seen from figure 11 that $\Phi$ decreases as $k_s/d$ increases. Although the value of $\tau_m/\rho V_0^2$ at large Reynolds numbers increases with increasing $k_s/d$ (see table 3 and figure 7 in Güven *et al.* 1977, specifically $\tau_m/\rho V_0^2 \simeq 0{\cdot}041(k_s/d)^{0{\cdot}2}$), this increase is more than off-set by the decrease in $\Phi$ and therefore $C_{ps}-C_{pm}$ decreases as $k_s/d$ increases. This is in accordance with the trends shown in figure 8.

It would be recalled that recourse was made to the extended Stratford–Townsend theory to describe, approximately, the boundary-layer behaviour in the region of pressure rise primarily owing to the failure of the detailed boundary-layer calculation procedures (specifically for surfaces with large relative roughness) beyond $\theta_m$. While the theory leads to a relatively simple relation involving the important parameters and explains the major trends observed from a wide range of experimental data, it does not by itself enable the prediction of, say, the drag coefficient or the major pressure distribution parameters such as $C_{pm}$ and $C_{pb}$, for a cylinder with known surface roughness at a given Reynolds number. A complete theoretical model would require a boundary-layer calculation procedure that can be relied upon to predict separation, and appropriate models for the wake and the external inviscid flow so that interactive solutions could be obtained. A first attempt at constructing such a model has been reported by Güven *et al.* (1977). There it is shown that such a model supports the large-Reynolds-number behaviour discussed in § 4.1 (*c*) (see also figure 8). In particular, the model indicates a marked insensitivity of the mean pressure distribution parameters to the location of boundary layer transition (which moves ahead with increasing $Re$ in the supercritical régime) if transition takes place at least a few degrees ahead of the position of the pressure minimum. For example, for $k_s/d = 10^{-5}$ and a free-stream turbulence intensity of 0·5 %, a change from $Re = 10^7$ to $Re = 10^8$ resulted in a shift in $\theta_t$ from 51 to 8 degrees, while the corresponding changes in $\tau_m/\rho V_0^2$, $\theta_w$, $C_{pb}$ and $C_{pm}$ were respectively from $4{\cdot}23 \times 10^{-3}$ to $4{\cdot}47 \times 10^{-3}$, 111·5 to 109 degrees, $-0{\cdot}62$ to $-0{\cdot}68$ and $-2{\cdot}04$ to $-1{\cdot}98$. A $Re$-independent condition is achieved when transition occurs sufficiently close to $\theta = 0$. The insensitivity for large supercritical $Re$ of the mean pressure distribution parameters (and of the wall shear stress at $\theta_m$) to the location of transition implies a similar insensitivity of these parameters to free-stream turbulence, at such large Reynolds numbers, if the main effect of free-stream turbulence is to shift the location of boundary-layer transition towards the stagnation point. In this connexion, it is interesting to note that insensitivity of mean pressure distributions to free-stream turbulence for moderate to high roughnesses is indicated by the rough-wall cooling tower experiments of Armitt (1968) in turbulent streams and by the agreement of Niemann's (1971) prototype results with those of cooling tower models operating in uniform 'turbulence-free' streams in the $Re$-independent range, reviewed by Farell, Güven & Maisch (1976). This problem still needs extensive fundamental work, in particular in connexion with the determination of turbulence-scale effects.

## 5. Conclusions

The present experimental results for circular cylinders in uniform streams, covering a somewhat limited range of Reynolds numbers, have been used together with previous data to explore the dependence of the mean drag coefficient and the major characteristic mean-pressure-distribution parameters, such as the pressure minimum, the base pressure, and the location of separation on Reynolds number and relative surface roughness. The main conclusions are summarized below.

(1) The drag coefficient, as well as the pressure-distribution parameters, become independent of Reynolds number as the Reynolds number is increased. The Reynolds-number-independent condition is achieved at lower Reynolds numbers as the surface-roughness increases. In the Reynolds-number-independent range, the drag coefficient, as well as the pressure-distribution parameters, show a definite dependence on the relative roughness. These conclusions confirm earlier results of Achenbach (1971, 1977).

(2) The observed variation of the drag coefficient and pressure-distribution parameters with relative surface roughness in the Reynolds-number-independent range may be explained on the basis of boundary layer behaviour. Specifically, it is shown that larger surface roughnesses lead to a thicker boundary layer with a larger momentum deficit which separates earlier, resulting in a smaller pressure rise ($C_{pb} - C_{pm}$) and a higher drag coefficient. The experimental observations are well supported by analytic considerations.

(3) In the evaluation of the effects of roughness, observations based on the drag-coefficient alone may in certain cases be misleading, as the drag-coefficient appears to be rather sensitive to factors such as length-to-diameter ratio, tunnel blockage, end conditions of the test cylinders, and side-wall conditions of the tunnel used. The non-dimensional pressure rise to separation, $C_{pb} - C_{pm}$, on the other hand, appears to be rather insensitive to such factors, as this study as well as others have indicated, and is primarily a function of relative roughness in the Reynolds-number-independent range. The dependence of $C_{pb} - C_{pm}$ on relative roughness is supported by the extension of the Stratford–Townsend theory of turbulent boundary-layer separation to the case of cylinders with distributed roughness, which is compared here with the experimental results.

(4) This study indicates that extensive fundamental research is still needed for a complete understanding of the complex flow around circular cylinders and the various factors which affect it.

The authors wish to acknowledge the assistance given by Professor J. R. Glover in the development of the computerized mean-pressure data acquisition system used in the experiments and by Mr Dale Harris and the IIHR workshop staff in the construction of the experimental apparatus. They also wish to express their gratitude to Dr Elmar Achenbach who kindly provided his detailed unpublished pressure-distribution data and to Dr Edmond Szechenyi who made available some necessary numerical values and information related to his data. The referees of the paper have also made valuable contributions and these are gratefully acknowledged. This paper is based upon research sponsored by the U.S. National Science Foundation under Grants no. GK-35795, ENG 76-08849 and ENG 78-22092.

## REFERENCES


ACHENBACH, E. 1968 Distribution of local pressure and skin friction around a circular cylinder in cross-flow up to $Re = 5 \times 10^6$. *J. Fluid Mech.* **34**, 625.

ACHENBACH, E. 1971 Influence of surface roughness on the crossflow around a circular cylinder. *J. Fluid Mech.* **46**, 321.

ACHENBACH, E. 1977 The effect of surface roughness on the heat transfer from a circular cylinder to the cross flow of air. *Int. J. Heat Mass Transfer.* **20**, 359.

ARMITT, J. 1968 The effect of surface roughness and free stream turbulence on the flow around a model cooling tower at critical Reynolds numbers. *Proc. Symp. on Wind effects on Buildings and Structures.* Loughborough University of Technology.

BATHAM, J. P. 1973 Pressure distributions on circular cylinders at critical Reynolds numbers. *J. Fluid Mech.* **57**, 209.

BEARMAN, P. W. 1969 On vortex shedding from a circular cylinder in the critical Reynolds number regime. *J. Fluid Mech.* **37**, 577.

DVORAK, F. A. 1969 Calculation of turbulent boundary layers on rough surfaces in pressure gradient. *A.I.A.A. J.* **7**, 1752.

FAGE, A. 1929 The air flow around a circular cylinder in the region where the boundary layer separates from the surface. *Aero. Res. Comm.* 1179.

FAGE, A. & WARSAP, J. H. 1929 The effects of turbulence and surface roughness on the drag of a circular cylinder. *Aero. Res. Comm.* 1283.

FARELL, C. 1971 On the modelling of wind loading on large cooling towers. *Proc. 2nd Ann. Thermal Power Conf. 5th Biennial Hydraul. Conf.*, p. 139. Washington State University, Pullman, Washington.

FARELL, C., CARRASQUEL, S., GÜVEN, O. & PATEL, V. C. 1977 Effect of tunnel walls on the flow past circular cylinders and cooling tower models. *Trans. A.S.M.E.* I, *J. Fluids Engng* **99**, 470.

FARELL, C., GÜVEN, O. & MAISCH, F. 1976 Mean wind loading on rough-walled cooling towers. *A.S.C.E. J. Engng Mech. Div.* **102**, no. EM6, 1059.

FARELL, C., GÜVEN, O. & PATEL, V. C. 1976 Laboratory simulation of wind loading of rounded structures. *Proc. I.A.S.S. World Cong. on Space Enclosures.* Montreal.

FARELL, C. & MAISCH, E. F. 1974 External roughness effects on the mean wind pressure distribution on hyperbolic cooling towers. *Iowa Inst. Hydraul. Res. Rep.* no. 164.

FEINDT, E. G. 1957 Untersuchungen uber die Abhangigkeit des Umschlages Laminarturbulent von der Oberflachenrauhigkeit und der Druckverteilung. *Jb. Schiffbautech. Ges.* **50**, 180.

GÜVEN, O. 1975 An experimental and analytical study of surface-roughness effects on the mean flow past circular cylinders. Ph.D. thesis, University of Iowa.

GÜVEN, O., PATEL, V. C. & FARELL, C. 1975*a* Surface roughness effects on the mean flow past circular cylinders. *Iowa Inst. Hydraulic Res. Rep.* no. 175.

GÜVEN, O., PATEL, V. C. & FARELL, C. 1975*b* Appendix 2 to *Iowa Inst. Hydraul. Res. Rep.* no. 175.

GÜVEN, O., PATEL, V. C. & FARELL, C. 1977 A model for high-Reynolds-number flow past rough-walled circular cylinders. *Trans. A.S.M.E.* I, *J. Fluids Engng* **99**, 486.

HALL, O. J. & GIBBINGS, J. C. 1972 Influence of stream turbulence and pressure gradient upon boundary-layer transition. *J. Mech. Eng. Sci.* **14**, 134.

HEAD, M. R. 1958 Entrainment in the turbulent boundary layers. *Aero. Res. Counc. R. & M.* 3152.

JONES, G. W., CINCOTTA, J. J. & WALKER, R. W. 1969 Aerodynamic forces on a stationary and oscillating circular cylinder at high Reynolds numbers. *N.A.S.A. Tech. Rep.* R-300.

NIEMANN, H. J. 1971 On the stationary wind loading of axisymmetric structures in the transcritical Reynolds number region. *Inst. Konstruktiven Ingenieurbau, Ruhr-Univ. Bochum, Rep.* no. 71–2.

PATEL, V. C. 1968 The effects of curvature on the turbulent boundary layer. *Aero. Res. Counc. R. & M.* 3599.

PATEL, V. C., NAKAYAMA, A. & DAMIAN, R. 1974 Measurements in the thick turbulent boundary layer near the tail of a body of revolution. *J. Fluid Mech.* **63**, 345.

RICHTER, A. & NAUDASCHER, E. 1976 Fluctuating forces on a rigid circular cylinder in confined flow. *J. Fluid Mech.* **78**, 561.

ROSENHEAD, L. 1963 *Laminar Boundary Layers.* Oxford University Press.

ROSHKO, A. 1961 Experiments on the flow past a circular cylinder at very high Reynolds number. *J. Fluid Mech.* **10**, 345.

ROSHKO, A. 1970 On the aerodynamic drag of cylinders at high Reynolds number. *U.S.–Japan Res. Seminar on Wind Loads on Structures.* Honolulu.

STRATFORD, B. 1959 The prediction of separation of the turbulent boundary layer. *J. Fluid Mech.* **5**, 1.

SZECHENYI, E. 1974 Simulation de nombres de Reynolds élevés sur un cylindre en soufflerie. *La Recherche Aérospatiale* 1974–**3**, 155.

SZECHENYI, E. 1975 Supercritical Reynolds number simulation for two-dimensional flow over circular cylinders. *J. Fluid Mech.* **70**, 529.

TOWNSEND, A. A. 1962 The behaviour of a turbulent boundary layer near separation. *J. Fluid Mech.* **12**, 536.

VAN NUNEN, J. W. G., PERSOON, A. J. & TIJDEMAN, H. 1974 Pressures and forces on a circular cylinder in a cross flow at high Reynolds numbers. *IUTAM/IAHR Symp. on Flow-Induced Structural Vibrations*, p. 748. Springer. (Also *Nat. Aero. Lab. Rep.* NLR TR 69102 U, Nederland, prepared for the European Space Vehicle Launcher Development Organization ELDO.)